Journal of Theoretical Biology 501 (2020) 110346

Contents lists available at ScienceDirect

Journal of Theoretical Biology

journal homepage: www.elsevier.com/locate/yjtbi

Phantom bursting may underlie electrical bursting in single pancreatic β-cells

Mehran Fazli [a], Theodore Vo [b], Richard Bertram [c,*]

[a] Florida State University, Department of Mathematics, Tallahassee, FL, United States
[b] Monash University, School of Mathematics, Clayton, Victoria, Australia
[c] Florida State University, Department of Mathematics and Programs in Neuroscience and Molecular Biophysics, Tallahassee, FL, United States

ARTICLE INFO

Article history:
Received 6 January 2020
Revised 18 May 2020
Accepted 23 May 2020
Available online 4 June 2020

Keywords:
Fast-slow analysis
Oscillations
Islet
Electrical activity
Glycolytic oscillations

ABSTRACT

Insulin is secreted by pancreatic β-cells that are electrically coupled into micro-organs called islets of Langerhans. The secretion is due to the influx of Ca^{2+} ions that accompany electrical impulses, which are clustered into bursts. So-called "medium bursting" occurs in many β-cells in intact islets, while in other islets the β-cells exhibit "slow bursting", with a much longer period. Each burst brings in Ca^{2+} that, through exocytosis, results in insulin secretion. When isolated from an islet, β-cells behave very differently. The electrical activity is much noisier, and consists primarily of trains of irregularly-timed spikes, or fast or slow bursting. Medium bursting, so often seen in intact islets, is rarely if ever observed. In this study, we examine what the isolated cell behavior can tell us about the mechanism for bursting in intact islets. A previous mathematical study concluded that the slow bursting observed in isolated β-cells, and therefore most likely in islets, must be due to intrinsic glycolytic oscillations, since this mechanism for bursting is robust to noise. It was demonstrated that an alternate mechanism, phantom bursting, was very sensitive to noise, and therefore could not account for the slow bursting in single cells. We re-examine these conclusions, motivated by recent experimental and mathematical modeling evidence that slow bursting in intact islets is, at least in many cases, driven by the phantom bursting mechanism and not endogenous glycolytic oscillations. We employ two phantom bursting models, one minimal and the other more biophysical, to determine the sensitivity of medium and slow bursting to electrical current noise. In the minimal model, both forms of bursting are highly sensitive to noise. In the biophysical model, while medium bursting is sensitive to noise, slow bursting is much less sensitive. This suggests that the slow bursting seen in isolated β-cells may be due to a phantom bursting mechanism, and by extension, slow bursting in intact islets may also be driven by this mechanism.

1. Introduction

Insulin is responsible for glucose uptake and utilization by muscle, liver, and adipose cells, and its secretion by pancreatic β-cells is regulated by blood glucose and various hormones and neurotransmitters (Rorsman and Ashcroft, 2018). The blood insulin level is pulsatile in non-diabetic humans and animals, and this pulsatility is an important factor in glucose homeostasis (Matthews et al., 1983; Satin et al., 2015). The oscillatory insulin level is known to reflect pulses of insulin secretion from islet β-cells, and is due to bursting electrical activity (Barbosa et al., 1998; Bergsten, 1995). Each burst of electrical impulses brings Ca^{2+} into the cell through Ca^{2+} channels, evoking Ca^{2+}-mediated exocytosis of insulin-containing granules. Thus, bursting produces periodic elevations in the intracellular Ca^{2+} concentration, resulting in pulses of insulin secretion.

Many electrical and Ca^{2+} recordings from islets have been published over several decades. In the vast majority of cases, islets exposed to stimulatory levels of glucose exhibit either "medium bursting" with period of roughly 15 s (Atwater et al., 1978; Cook et al., 1980), or "slow bursting" with longer periods of up to 5 min (Valdeolmillos et al., 1989; Zhang et al., 2003). Interestingly, islets from the same mouse tend to have similar burst periods, either all medium or all slow (Nunemaker et al., 2005). The mechanism for these oscillations has been under investigation since the 1970's, aided by mathematical modeling since the first-published model in 1983 (Chay and Keizer, 1983). One mechanism for both forms of bursting, "phantom bursting", involves the actions of two slow processes with very different time scales, acting together on the cell's membrane potential to package electrical impulses

* Corresponding author.
E-mail address: bertram@math.fsu.edu (R. Bertram).

https://doi.org/10.1016/j.jtbi.2020.110346
0022-5193/

into bursts. Bursting can be produced with a period that is close to either time constant, or anything in between, depending on key parameter values, and so there is a wide range of burst periods. This provides a great deal of flexibility, and variation of a single ion channel conductance can produce bursts with periods ranging from tens of seconds to several minutes (Bertram et al., 2000).

For slow bursting, a second mechanism has been postulated by Tornheim in 1997 (Tornheim, 1997), and is based on the ability of a key allosteric enzyme in the glycolytic pathway to produce oscillations with a period similar to that of slow bursting and pulsatile insulin secretion. This enzyme, phosphofructokinase (PFK), was shown to produce oscillations in its substrate (fructose 6-phosphate, F6P) and in its product (fructose 1,6-bisphosphate, FBP) in muscle extracts (Tornheim and Lowenstein, 1973; Tornheim and Lowenstein, 1974). The same M-type isoform is prevalent in β-cells (Yaney et al., 1995). This "glycolytic mechanism" for slow bursting was later incorporated into a biophysical β-cell model, the Dual Oscillator Model (DOM) (Bertram et al., 2004), as the basis for slow bursting as well as "compound bursting", which consists of episodes of fast bursts clustered together into episodes (Cook, 1983; Henquin et al., 1982) by the glycolytic oscillator.

With these two potential driving mechanisms for slow bursting, a natural question is which, if either, is correct. This was addressed in a novel way by examining how each of the mechanisms holds up to noise (Pedersen, 2007). *In vivo*, the β-cells are coupled together by gap junctions into pancreatic islets of Langerhans; because of this electrical coupling the cells act as a syncytium, all cells sharing their combined membrane and oscillating together. In this physiological network, channel noise has little impact on the membrane potential since the membrane (and number of channels) is so large (Sherman et al., 1988). However, in single β-cells that are isolated from an islet, the very small cells ($\sim$ 10 μm in diameter) exhibit a very noisy voltage time course, reflecting the much smaller membrane area (Kinard et al., 1999; Zhang et al., 2003). Pedersen showed that a simple model for phantom bursting was very vulnerable to noise, so that medium bursting in the deterministic model was replaced by noisy "fast bursting" (with period of a few seconds). Slow bursting with the phantom bursting model was not examined, but slow bursting driven by glycolytic oscillations was shown to be robust to noise (Pedersen, 2007). These results are important, since they show why medium bursting is never observed in single cells, and they suggest that any slow bursting or slow Ca^{2+} oscillations observed in single cells are due to glycolytic oscillations (Pedersen, 2007). One can also extrapolate from this that slow bursting and Ca^{2+} oscillations in intact islets is likely due to glycolytic oscillations.

In this report we re-examine the question of whether phantom bursting is sensitive to noise. This is motivated by a recent experimental study that used a FRET (Föster Resonance Energy Transfer) sensor along with Ca^{2+} imaging to show that the FBP time course in islets that exhibit slow Ca^{2+} oscillations has the shape of a triangle wave (Merrins et al., 2016). This is contrary to what would be expected if intrinsic glycolytic oscillations were occurring, where the FBP concentration would exhibit pulses (McKenna et al., 2016). It is, however, consistent with a phantom bursting mechanism (McKenna and Bertram, 2018). Given this, one would expect that at least in some cases the slow Ca^{2+} oscillations and slow electrical bursting observed in isolated β-cells should be driven by a phantom mechanism, contrary to the conclusion of Pedersen (2007).

We begin by examining a minimal model for phantom bursting (Bertram et al., 2000), and demonstrate that both medium and slow bursting produced by this model are sensitive to electrical current noise (which reflects the stochastic gating of ion channels). We then progress to a more recent, and more biophysical, model called the Integrated Oscillator Model (IOM) (Marinelli et al., 2018). As with the minimal model, medium bursting produced by the IOM is sensitive to noise. However, slow bursting driven by a phantom mechanism in the model is much less sensitive. To understand these findings we employ fast-slow analysis and examine the fast-subsystem properties in the phase plane. We conclude that the slow electrical bursting and Ca^{2+} oscillations observed in single β-cells, where the environment is inherently noisy, could be driven by either a phantom bursting mechanism or, as proposed in Pedersen (2007), by intrinsic glycolytic oscillations.

2. Medium and slow bursting are sensitive to noise in a minimal phantom bursting model

The minimal phantom bursting model was developed specifically to demonstrate how a model of cell electrical activity with two slow processes operating on very different time scales can produce a wide range of burst periods (Bertram et al., 2000). It consists of a differential equation for the membrane potential or voltage (V), another for the fraction of activated delayed-rectifier-type K^+ -channels (n), and two slower activation variables (s_1 and s_2) for two additional types of K^+ channels. The differential equations are:

$$\frac{dV}{dt} = -(I_{Ca} + I_K + I_{s1} + I_{s2} + I_L + I_{noise})/C_m \tag{1}$$

$$\frac{dn}{dt} = \frac{n_\infty(V) - n}{\tau_n(V)} \tag{2}$$

$$\frac{ds_1}{dt} = \frac{s_{1\infty}(V) - s_1}{\tau_{s1}} \tag{3}$$

$$\frac{ds_2}{dt} = \frac{s_{2\infty}(V) - s_2}{\tau_{s2}} \,. \tag{4}$$

The three activation variables change on very different time scales: $\tau_n(V) < 10$ ms, $\tau_{s1} = 1$ s, and $\tau_{s2} = 2$ min, so $\tau_n \ll \tau_{s1} \ll \tau_{s2}$. The n variable dynamics are responsible for the downstroke of action potentials, while s_1 and s_2 package action potentials into bursts (Bertram et al., 2000). With the exception of I_{noise}, expressions for the ionic currents and other functions are identical to those given in Bertram et al. (2000), and the computer code can be downloaded from www.math.fsu.edu/bertram/software/islet. Brownian noise is added to the voltage through the current

$$I_{noise} = \sigma w \sqrt{dt} \tag{5}$$

where w is a Wiener variable and σ is an amplitude parameter. When noise is present, we set $\sigma = 300$ fA, and otherwise $\sigma = 0$. The differential equations are solved numerically using the Euler method with time step $\Delta t = 0.1$ ms.

The s_1 current is critical to setting the burst period, so we give it here:

$$I_{s1} = g_{s1} s_1 (V - V_K) \tag{6}$$

where g_{s1} is the maximal conductance of the current and V_K is the K^+ Nernst potential. When g_{s1} is large the s_1 current is of sufficient size to drive bursting, so the bursting is fast. When g_{s1} is small, the s_1 current is insufficient to terminate spiking and there must be a substantial contribution from the s_2 current (the size of the contribution has an inverse relationship with the size of g_{s1} (Watts et al., 2011)). Since s_2 changes on a much slower time scale, bursting in this case is much slower. Thus, by varying the parameter g_{s1} one can readily vary the burst period over a wide range of values. The flexibility of burst periods exhibited by the minimal model is illustrated in Fig. 1. In panel A, the burst period is a few seconds (fast

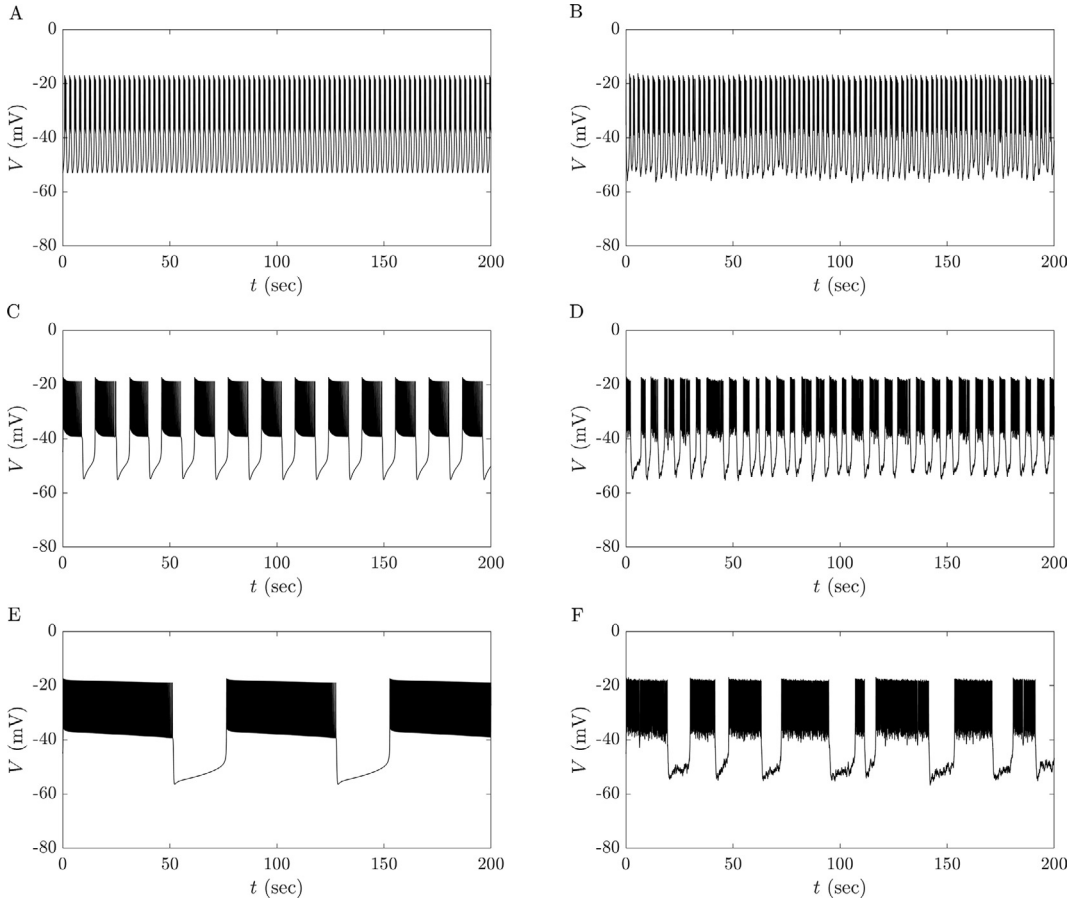

Fig. 1. Bursting produced by the minimal phantom bursting model for β-cell activity. (A) Fast bursting, with $g_{s1} = 20$ pS. (B) There is little change in the fast bursting when noise is added. (C) Medium bursting, with $g_{s1} = 7$ pS. (D) The burst period is substantially reduced when noise is added. (E) Slow bursting, with $g_{s1} = 3$ pS. (F) The burst period is again substantially reduced when noise is added.

bursting), in panel C it is approximately 15 s (medium bursting), and in panel E it is approximately 80 s (slow bursting).

The introduction of noise brings about significant changes. The fast bursting remains fast (panel B), but the burst periods for medium (panel D) and slow bursting (panel F) are significantly reduced. Apparently, both of these forms of bursting are sensitive to noise. This is quantified in Fig. 2. Panels A and B are histograms characterizing 100 active phase durations (A) and silent phase durations (B) computed using the model with noise. These durations are normalized by the active (silent) phase duration of the burst attractors of the deterministic model. The histograms for what would be medium bursting in the deterministic case are shown in blue, while those for slow bursting are in red. These illustrate that many noisy bursts have active and silent phase durations less than half as long as the deterministic bursts, for both medium and slow bursting. These data are used to compute cumulative probability distributions that are shown in panels C and D. In panel C, for example, the fraction of active phases in the noisy model simulation with relative duration (i.e., relative to the deterministic case) less than X is plotted for a sampling of $X \leqslant 1$. For both medium and slow bursting, roughly 80% of the active phases are less than half the duration of the deterministic active phases. For the silent phases, roughly 40% are less than half as long as the deterministic silent phases for medium bursting, while the percentage is closer to 70% for slow bursting.

This analysis indicates that both medium and slow bursting are sensitive to noise, though slow bursting appears to be somewhat more sensitive (bars in Fig. 2B, D are more left shifted for slow bursting than for medium bursting). Since both forms of bursting are produced through a phantom bursting mechanism, i.e., they require significant changes in both s_1 and s_2 to achieve the bursting pattern, this result is consistent with the prior study that used a different minimal phantom bursting model (Pedersen, 2007).

3. Slow bursting is only moderately sensitive to noise in a biophysical β-cell model

The Integrated Oscillator Model (IOM) was developed over a period of many years based on a number of key experimental findings (Bertram et al., 2018), and includes modules for electrical activity, intracellular Ca^{2+} handling, and metabolism. In this model, fast and medium bursting are driven by Ca^{2+} feedback onto Ca^{2+}-activated K^+ channels; in the case of medium bursting significant variation in the Ca^{2+} concentration in the endoplasmic reticulum (ER) is also required, as described in Bertram and Sherman (2004). Slow bursting can be produced in one of two ways. In one case, there are active metabolic oscillations due to positive feedback onto the allosteric enzyme phosphofructokinase in glycolysis. This substrate depletion mechanism for oscillations drives the oscillations in electrical activity and Ca^{2+} through the action of ATP-sensitive K^+ channels (K(ATP) channels). These channels are deactivated when the ratio of adenosine triphosphate (ATP) to adenosine diphosphate (ADP) is increased; active oscillations in glycolysis lead to ATP/ADP oscillations, which cause slow bursting oscillations via ionic current through the K(ATP) channels. This

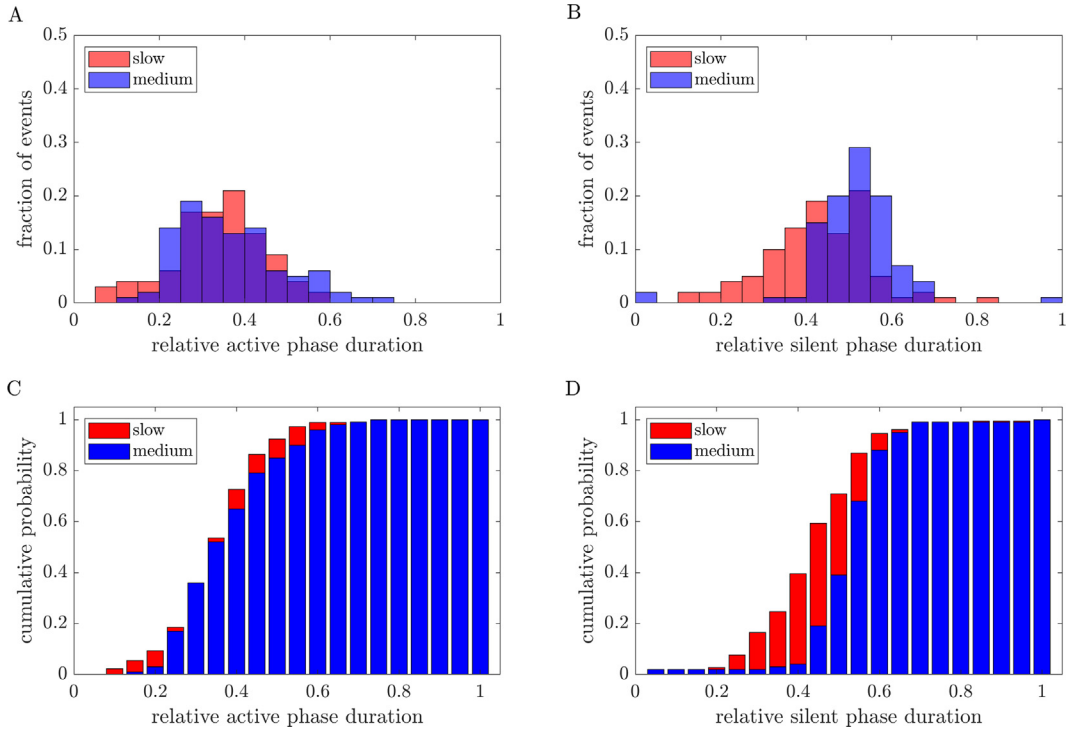

Fig. 2. Quantification of the effects of noise on medium and slow bursting in the minimal phantom bursting model. (A) Histogram of 100 events showing the active phase duration relative to that of the deterministic model. Medium bursting is shown in blue, while slow bursting is shown in red. The effects of noise on the active phase duration are similar in both types of bursting. (B) Histogram of 100 events showing the silent phase duration relative to that of the deterministic model. The effects of noise on the silent phase duration are similar in both types of bursting. (C-D) Data from panels A and B plotted as cumulative probability distributions.

was the mechanism for slow bursting studied in a previous report, and shown to be relatively insensitive to noise (Pedersen, 2007).

The other mechanism for slow bursting in the IOM occurs when the flux out of glycolysis is sufficiently small (Marinelli et al., 2018). This flux is set by the maximum catalytic rate of pyruvate dehydrogenase (v_{PDH}). With a small value of v_{PDH} the metabolic oscillations are purely passive, slaved to oscillations in the intracellular Ca^{2+} concentration. These Ca^{2+} oscillations influence the ATP/ADP ratio through positive feedback onto metabolism (increasing ATP production) and negative feedback through the hydrolysis needed to power Ca^{2+} pumps (increasing ATP consumption) (Bertram et al., 2018; McKenna et al., 2016; Marinelli et al., 2018). It has been shown that this form of slow bursting, with passive metabolic oscillations, is due to a phantom bursting mechanism involving the ATP concentration and the Ca^{2+} concentration in the ER (McKenna and Bertram, 2018).

As with the minimal phantom bursting model, changes in a single conductance parameter are sufficient to convert the bursting between fast, to medium, to slow. This is the conductance for Ca^{2+}-activated K^+ channels, $g_{K(Ca)}$, in the ionic current equation

$$I_{K(Ca)} = g_{K(Ca)} q_\infty(c)(V - V_K) \tag{7}$$

where

$$q_\infty(c) = \frac{c^2}{k_d^2 + c^2} \tag{8}$$

and c is the free cytosolic Ca^{2+} concentration. The full model is described in Marinelli et al. (2018) and computer code can be downloaded from www.math.fsu.edu/bertram/software/islet.

Examples of fast, medium, and slow bursting generated by the IOM are shown in Fig. 3. The fast bursting is generated using a large value of $g_{K(Ca)}$, while slower forms of bursting use smaller values of the parameter. The slow bursting does not involve an active glycolytic oscillator; metabolic oscillations are slaved to Ca^{2+} oscillations and are passive. With the addition of noise in the V differential equation, the period of all forms of bursting is reduced. However, the effect of noise on medium bursting appears to be more extreme than that on slow bursting.

The effects of noise on medium and slow bursting in the IOM is quantified in Fig. 4. Panels A and B indicate that the noise shortens both active and silent phases of medium bursting to a substantially greater degree than it does the active and silent phases of slow bursting. There is a clear separation in the histograms for the two types of bursting, unlike the case with the minimal model (Fig. 2). In the cumulative probability panel C, we see that for medium bursting approximately half of the noisy active phases have duration less than 25% that of the deterministic model, while for slow bursting all active phases are greater than 25% of that of the deterministic model and most are greater than 50% that of the deterministic model. The difference is even more striking for silent phases. For medium bursting, approximately half of the noisy silent phases are less than 40% that of the deterministic model, while for slow bursting all noisy silent phase are greater than half of that of the deterministic model, and most are greater than 75% of the deterministic model. This quantification is consistent with Fig. 3, indicating that medium bursting with the IOM is more sensitive to the effects of noise than is slow bursting.

4. A phase plane explanation of the differential effects of noise on bursting

In both β-cell models discussed above, the variables can be partitioned into those that evolve on a fast time scale and those that evolve on a slower time scale. This partitioning is the first step in

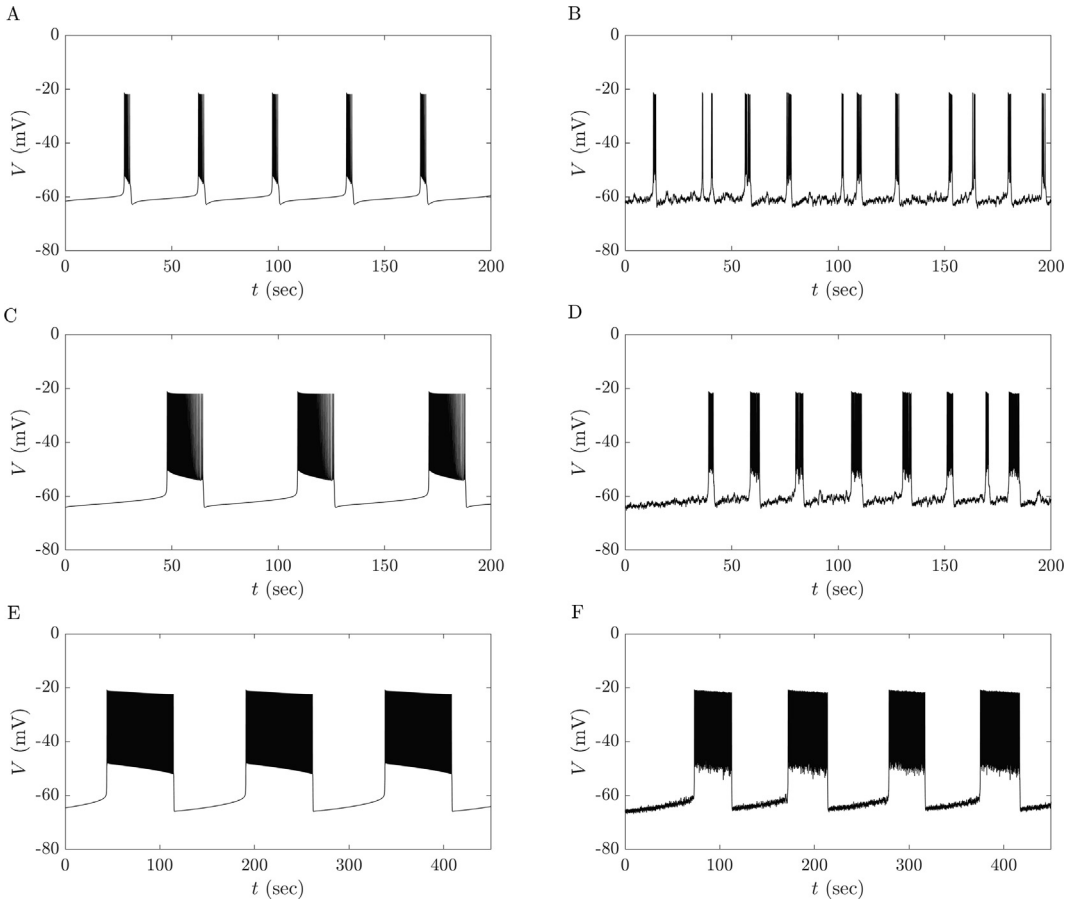

Fig. 3. Bursting produced by the Integrated Oscillator Model for β-cell activity. (A) Fast bursting, with $g_{K(Ca)} = 800$ pS. (B) Some bursts are converted to single spikes, and there is a reduction in the burst silent phase. The burst active phase is less affected by the noise. (C) Medium bursting, with $g_{K(Ca)} = 500$ pS. (D) The burst period is substantially reduced when noise is added, yielding shorter silent and active phases. (E) Slow bursting, with $g_{K(Ca)} = 100$ pS. (F) The noise has little effect on the burst period. In all cases, the pyruvate dehydrogenase parameter is set at $v_{PDH} = 0.002$ μM/ms and noise is introduced by setting $\sigma = 300$ fA.

a fast-slow analysis that is often used to understand multi-timescale systems (Bertram and Rubin, 2017). The evolution of the slow variables carries orbits through the asymptotic regimes of the fast subsystem, and determines whether the system is in a spiking state or at rest. Periodicity of the values of the slow variables produces bursting. Another key feature of both models is bistability of the fast subsystem between a stable equilibrium and a stable limit cycle for most values of the slow variables taken on during bursting. This is illustrated in Fig. 5, which shows structures for the fast subsystem (the V and n variables) in the minimal (deterministic) phantom bursting model. The values of the slow variables, s_1 and s_2, are chosen as those taken on 20% through the active phase of a medium burst. The V-nullcline (yellow) and n-nullcline (green) intersect at three locations. The first of these, E_1, is a stable node, while E_2 is a saddle point and E_3 is an unstable focus. Surrounding the focus is a stable limit cycle (red). Also shown are the two branches of the stable manifold (dashed blue) of the saddle that act as a separatrix between the two attractors. The limit cycle reflects spiking solutions of the subsystem, while the stable equilibrium reflects the state of the system during the burst silent phase. Since noise enters through the V differential equation, it directly affects the fast subsystem dynamics, causing upward or downward deflections in the trajectory. If the phase point is in the basin of attraction of the limit cycle, as it would be during the burst active phase, then if noise kicks the trajectory across the separatrix it will prematurally terminate the active phase. If the phase point is in the basin of attraction of E_1, as it would be during the burst silent phase, then if noise kicks the trajectory across the separatrix it will prematurally terminate the silent phase. Thus, one can understand the effects of noise in terms of the two stable structures and their distance from the separatrix. Fig. 6 shows, for the minimal phantom bursting model, structures of the fast subsystem phase plane for both medium (blue) and slow (red) bursting. Panel A shows the separatrices and action potential limit cycles with s_1 and s_2 values chosen 20% through a burst active phase (these values are different for medium and slow bursting). It is evident that, in both cases, the spiking limit cycle is close to the separatrix. In fact, the vertical distance between these structures during slow bursting is similar to that during medium bursting. (It is the vertical distance that is important since noise acts directly on the V variable.) It is for this reason that the noise sensitivity of the active phase is similar in both forms of bursting. Panel B shows nullclines, separatrices, and equilibria with s_1 and s_2 values chosen 20% through a burst silent phase. In the case of medium (blue) and slow (red) bursting, the phase point is at or near equilibrium E_1 during the silent phase and the silent phase is prematurally terminated by noise if the noise displaces the phase point above the separatrix. The distance between E_1 and the separatrix is very similar in medium and slow bursting, so again the expectation is that sensitivity to noise of the silent phase is similar in both forms of bursting.

The fast subsystem of the IOM model again consists of the variables V and n, and Fig. 7 shows fast subsystem structures with slow variables set to their values 20% through the active phase of

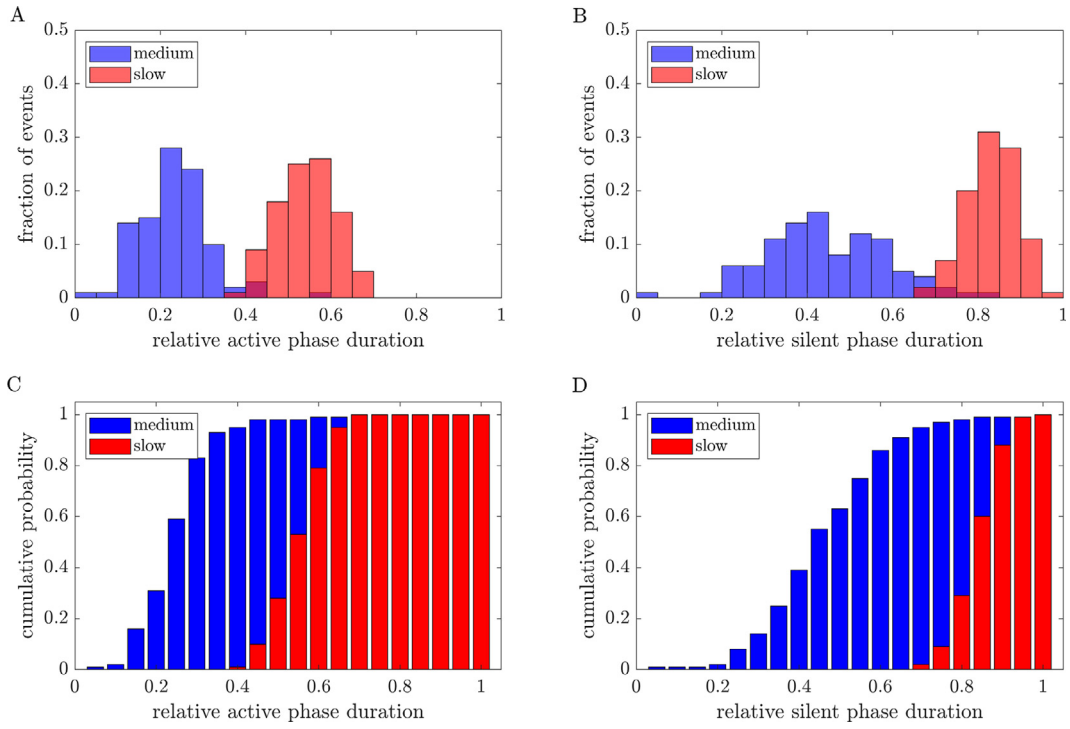

Fig. 4. Quantification of the effects of noise on medium and slow bursting in the Integrated Oscillator Model. (A) Histogram of 100 events showing the active phase duration relative to that of the deterministic model. Medium bursting is shown in blue, while slow bursting is shown in red. The effects of noise on the active phase duration of medium bursting are greater than for slow bursting. (B) Histogram of 100 events showing the silent phase duration relative to that of the deterministic model. The effects of noise on the silent phase duration of medium bursting are greater than for slow bursting. (C, D) Data from panels A and B plotted as cumulative probability distributions.

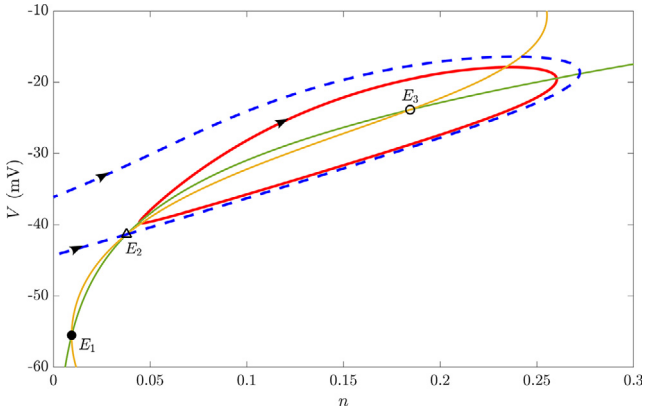

Fig. 5. Fast subsystem phase plane of the minimal model. The V-nullcline (yellow) and n-nullcline (green) intersect to form three equilibria. Equilibrium E_1 is a stable node, E_2 is a saddle point, and E_3 is an unstable focus. The limit cycle (red) is stable. The two branches of the stable manifold of E_2 form the separatrix between the basins of attraction of the two stable structures. The values of the slow variables s_1 and s_2 are those taken on 20% of the way through the active phase of medium bursting: $s_1 = 0.63$ and $s_2 = 0.60$, with $g_{s1} = 7$ pS. (For interpretation of the references to colour in this figure legend, the reader is referred to the web version of this article.)

medium bursting. (The slow variables that directly affect the fast subsystem are cytosolic Ca^{2+} concentration, c, and ADP level, ADP.) The fast variable nullclines are similar to those of the minimal model, and again cross to form three labeled equilibria.The single stable equilibrium, E_1, coexists with a stable limit cycle (solid blue), and the separatrix for the basins of attraction is formed by the two branches of the stable manifold of E_2 (dashed blue). The similarity to Fig. 5 illustrates that the fast subsystem structure for the two models is qualitatively similar.

The spiking orbit 20% through the active phase of medium bursting (solid blue) is shown superimposed with that 20% through slow bursting (solid red) in Fig. 8A. The separatrices are also shown, as dashed curves. It is evident that the spiking orbit is closer to the separatrix during medium bursting than during slow bursting. This suggests that noise will be more likely to prematurally terminate an active phase during medium bursting than it would during slow bursting. Indeed, Fig. 4 shows that approximately 30% of the noisy medium bursts had active phases that were 20% or less of their deterministic duration, while few if any of the noisy slow burst active phases were 20% or less of their deterministic duration. Fig. 8B shows the nullclines and equilibria 20% through the silent phase of medium (blue) and slow (red) bursting. In these cases, both E_1 and E_2 are nearly at the same values of n, so if noise perturbs the phase point to a V value greater than that of E_2 the silent phase will be prematurally terminated. It is evident that E_1 and E_2 are much closer together for the case of medium bursting than for the case of slow bursting. For this reason, the silent phase of medium bursting is more sensitive to noise than is that of slow bursting. In summary, Fig. 8 demonstrates why in the IOM medium bursting is more sensitive to noise than is slow bursting, as shown by the histograms in Fig. 4.

At which point on the spiking limit cycle is it most likely that noise will push the trajectory across the separatrix into the basin of attraction of E_1, terminating a burst active phase? From Fig. 7 it appears that this might be along the top portion of the limit cycle, which is closest to the separatrix and is the peak of an action potential. To investigate whether this is true, we superimpose a noisy fast subsystem trajectory onto the fast subsystem phase plane diagram in Fig. 9 (using parameter values and values of c and ADP from Fig. 7). This noisy spiking trajectory (shown in black) moves away from the limit cycle with each revolution, due to the effects of the noise. It crosses the separatrix not at the top of the limit cycle, but in the bottom portion, denoted by a green dot.

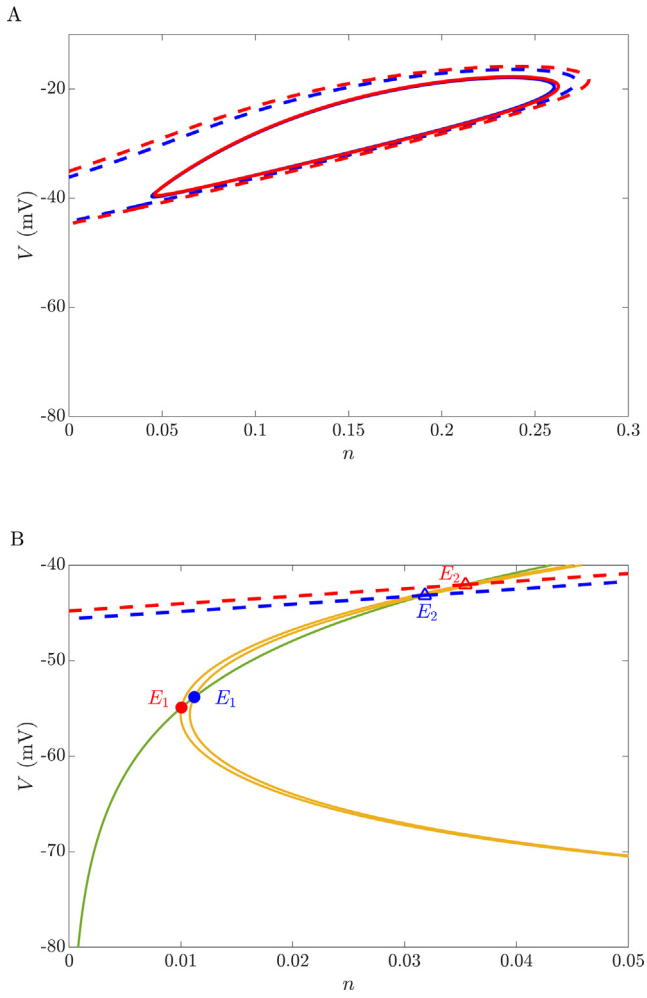

Fig. 6. Phase planes of the fast subsystem explain why medium and slow bursting have similar sensitivities to noise in the minimal phantom bursting model. (A) Limit cycles reflecting spiking orbits during the active phases of medium (solid blue) and slow (solid red) bursting are superimposed, along with separatrices (i.e., stable manifolds of E_2) for each (dashed). The distance between the limit cycle and separatix is similar for medium and slow bursting. Equilibria are not shown. In both cases, s_1 and s_2 are chosen at values 20% through the burst active phase. Medium bursting: $s_1 = 0.63$ and $s_2 = 0.60$, with $g_{s1} = 7$ pS. Slow bursting: $s_1 = 1$ and $s_2 = 0.63$, with $g_{s1} = 3$ pS. (B) Nullclines, equilibria, and separatrices at values of the slow variables 20% through a burst silent phase. The distance from E_1 to the separatrix is similar for medium and slow bursting. Medium bursting: $s_1 = 0.26$ and $s_2 = 0.63$, with $g_{s1} = 7$ pS. Slow bursting: $s_1 = 0.01$ and $s_2 = 0.72$, with $g_{s1} = 3$ pS. (For interpretation of the references to colour in this figure legend, the reader is referred to the web version of this article.)

Nineteen additional stochastic spiking trajectories were computed, and the location at which each crosses the separatrix is indicated with a orange dot in the figure. (Each dot is the location where a stochastic spiking trajectory leaves the basin of attraction of the limit cycle and does not return.) It is evident that in only one instance did the trajectory escape the spiking basin of attraction near the top of the limit cycle; in all other instances the escape occurred near the bottom of the limit cycle, during the repolarized phase of the action potential. In fact, the escape often occurred close to the saddle point, E_2.

Why does a noisy trajectory usually escape the spiking basin of attraction near the bottom of the limit cycle rather than the top? To answer this, we first consider the proximal effect of a noisy current (in contrast to long-term effects which can cause the phase point to switch basins of attraction) on the membrane potential. The voltage time derivative is proportional to the sum of the ionic

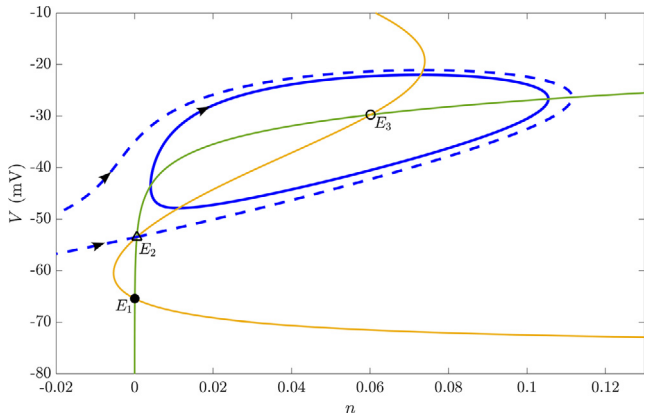

Fig. 7. Fast subsystem phase plane for the IOM. The V-nullcline (yellow) and n-nullcline (green) intersect to form three equilibria. Equilibrium E_1 is a stable node, E_2 is a saddle point, and E_3 is an unstable focus. The limit cycle (solid blue) is stable. The two branches of the stable manifold of E_2 (dashed blue) form the separatrix between the basins of attraction of the two stable structures. The values of the slow variables are those taken on 20% of the way through the active phase of medium bursting: $c = 0.11$ μM and ADP $= 807$ μM, with $g_{K(Ca)} = 500$ pS. Here and in subsequent phase plane figures the range of n extends to negative values. This is for visualization purposes only; for appropriate initial conditions, n only takes on values from 0 to 1. (For interpretation of the references to colour in this figure legend, the reader is referred to the web version of this article.)

currents, which we denote as I_{ion}, plus the noisy current, I_{noise}. The effect of noise on $\frac{dV}{dt}$ is thus determined by the size of I_{noise} relative to the total current, the sum of I_{ion} and I_{noise}. We therefore define the relative noise as

$$\eta = \frac{|I_{\text{noise}}|}{|I_{\text{ion}} + I_{\text{noise}}|} \tag{9}$$

and examine how this varies throughout the fast subsystem phase plane.

The current noise can either be depolarizing, causing an upward deflection in V, or repolarizing, causing a negative deflection. We consider each case separately. Fig. 10A shows a heat map of $\log_{10}(\eta)$ applied at points throughout the V-n phase plane where the noise is depolarizing (positive). At each point in the V-n plane, we set I_{noise} to be the mean of the positive noise values calculated over a stochastic spiking trajectory. The relative noise is greatest in the green and blue regions of the diagram, which take on the cubic shape of the V nullcline (where $I_{\text{ion}} = 0$), although this nullcline is located slightly to the right in the green-yellow region. Although the relative positive noise is large near the peak of the action potential (largest value of V) and is of the correct sign to push the trajectory across the separatrix, this only happens rarely (1 of the 20 stochastic simulations performed, shown as a blue point in upper portion of the diagram). At the bottom portion of the action potential limit cycle the positive current noise pushes the trajectory away from the separatrix, so will not contribute to the resetting.

Fig. 10B shows a heat map of $\log_{10}(\eta)$ where the noise is repolarizing (negative). Most of the 20 points at which noisy spiking trajectories crossed through the separatrix (blue points on the dashed white separatrix) occur in a region where the relative noise is large. This region is located primarily near the bottom of the limit cycle, and it is in this region that repolarizing noise is most effective at perturbing the trajectory down and away from the limit cycle. From a biophysical perspective, this is not surprising, since the repolarized phase of the action potential is when most ion channels are deactivated, so noise (or any other input) will have the largest effect on the membrane potential.

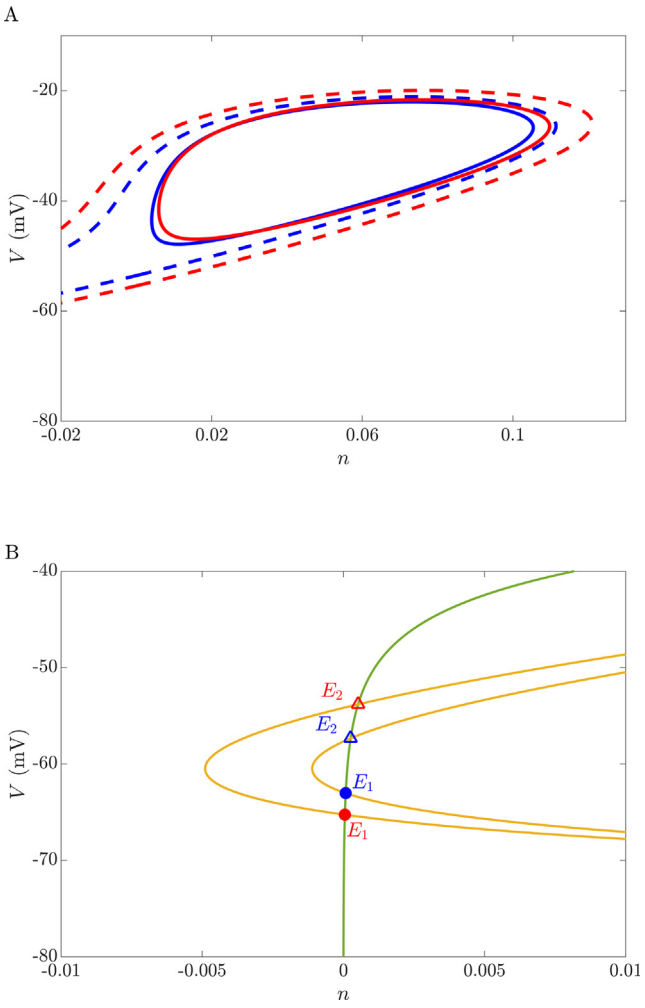

Fig. 8. Fast subsystem phase plane for the IOM. (A) Spiking limit cycles for medium (solid blue) and slow (solid red) bursting are superimposed, along with separatrices for each (dashed). The distance between the limit cycle and separatix is less for medium bursting than for slow bursting. In both cases, the slow variables c and ADP are chosen at values 20% through the burst active phase. Equilibria are not shown. Medium bursting: $c = 0.11$ μM and ADP = 807 μM, with $g_{K(Ca)} = 500$ pS. Slow bursting: $c = 0.16$ μM and ADP = 842 μM, with $g_{K(Ca)} = 100$ pS. (B) Nullclines and equilibria at values of the slow variables 20% through a burst silent phase. The distance from E_1 to the threshold E_2 is smaller for medium bursting than for slow bursting. Medium bursting: $c = 0.08$ μM and ADP = 812 μM, with $g_{K(Ca)} = 500$ pS. Slow bursting: $c = 0.11$ μM and ADP = 872 μM, with $g_{K(Ca)} = 100$ pS. (For interpretation of the references to colour in this figure legend, the reader is referred to the web version of this article.)

Why were there so few resettings with depolarizing current noise near the peak of the action potential? To answer this, the limit cycle is depicted not as a solid curve in Fig. 10, but as points plotted at equally spaced times. It is evident that the points accumulate near the bottom of the limit cycle, indicating that the trajectory is moving more slowly here. The slower the trajectory is moving, the greater the opportunity for noise to push the trajectory across the separatrix, so the explanation for the minimal effect of depolarizing noise during the top portion of the action potential is simply that the trajectory is moving quickly through this portion of the limit cycle (and this is reflected by the fixed stepsize numerical scheme that we use for the differential equations).

Taken together, these factors explain why the noisy spiking trajectory typically crosses the separatrix near the bottom of the limit cycle. From this, we can make a more precise statement regarding noise sensitivity during the active phase of medium and slow

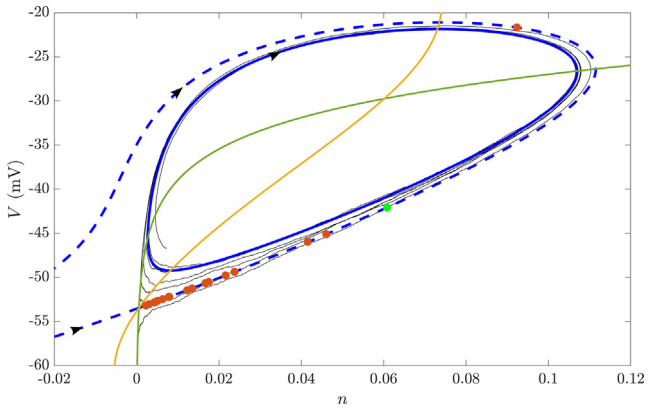

Fig. 9. Superposition of a fast subsystem stochastic spiking trajectory (black curve) onto the fast subsystem phase plane for the IOM 20% through the active phase of medium bursting ($c = 0.08$ μM and ADP = 812 μM, with $g_{K(Ca)} = 500$ pS). After several revolutions, the trajectory crosses the separatrix at the green dot. The orange dots show crossing points for 19 other stochastic spiking trajectories that leave the basin of attraction of the limit cycle and don't return. (For interpretation of the references to colour in this figure legend, the reader is referred to the web version of this article.)

bursting: if the distance between the bottom portion of the spiking limit cycle is closer to the separatrix in one form of bursting than another, then the former is more sensitive to current noise. The remainder of the limit cycle is much less important. We see from Fig. 8A that, by this criterion, medium bursting is more sensitive to noise than is slow bursting in the IOM, as was determined in Fig. 4A, C.

5. Noise reduces the burst plateau fraction

Pancreatic β-cells respond to changes in the blood glucose level by changing the burst plateau fraction, defined as the active phase duration divided by the full burst period (sum of the active and silent phase durations). In a bursting islet, increases in the glucose level cause the plateau fraction to increase, eventually reaching a value of 1 when the bursting is converted to tonic spiking (Meissner and Schmelz, 1976; Nunemaker et al., 2006). Higher plateau fractions result in higher mean Ca^{2+} levels and increased insulin secretion (Barbosa et al., 1998). How does noise affect the plateau fraction in the two β-cell models? Fig. 11A shows histograms of the plateau fraction for the medium and slow bursting in the minimal β-cell model. The dashed lines represent the plateau fraction for the deterministic cases (blue for medium bursting and red for slow bursting). It is evident that, with this model, the addition of noise results in a significant reduction in the plateau fraction for both forms of bursting. Fig. 11B shows plateau fraction histograms for medium and slow bursting in the IOM, along with deterministic values. Again, the addition of noise decreased the plateau fraction in both forms of bursting. That noise induces a reduction in the plateau fraction in all cases reflects the greater sensitivity of the active phase of bursting to noise than the silent phase in both models.

6. Slow bursting driven by an active metabolic oscillator is only moderately sensitive to noise

Pedersen showed that slow bursting driven by active metabolic oscillations produced in the Dual Oscillator Model is only moderately sensitive to noise (Pedersen, 2007). A similar type of slow bursting, driven by an active glycolytic oscillator, is produced by the IOM in a large region of parameter space (Marinelli et al., 2018). Indeed, by increasing the parameter v_{PDH} from 0.002 μM/ms

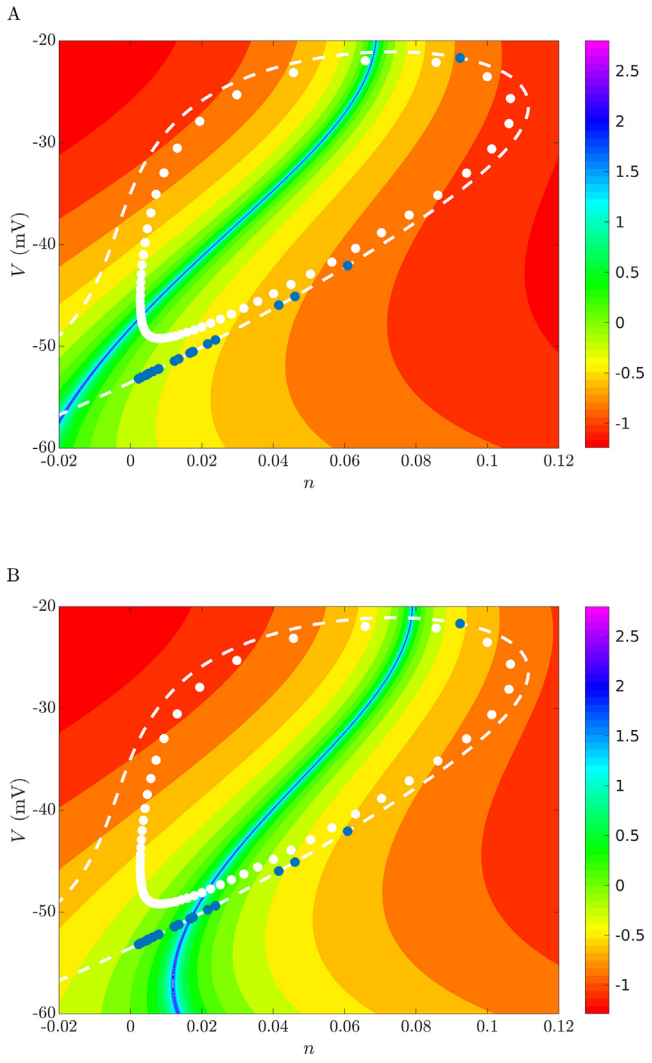

Fig. 10. (A) Heat map of $\log_{10}(\eta)$ with depolarizing (positive) current noise, and with superimposed phase plane structure of the fast subsystem for the IOM, 20% of the way through the active phase of medium bursting ($c = 0.08$ μM and ADP = 812 μM, with $g_{K(Ca)} = 500$ pS). The blue dots show crossing points for the 20 stochastic spiking trajectories through the separatrix (dashed white). The limit cycle is shown as white points, with equal spacing of $\Delta t = 2.5$ ms. (B) Heat map of $\log_{10}(\eta)$ with repolarizing (negative) current noise. Most resettings occur near the lower portion of the limit cycle where the relative repolarizing noise is large and the speed of passage is low. (For interpretation of the references to colour in this figure legend, the reader is referred to the web version of this article.)

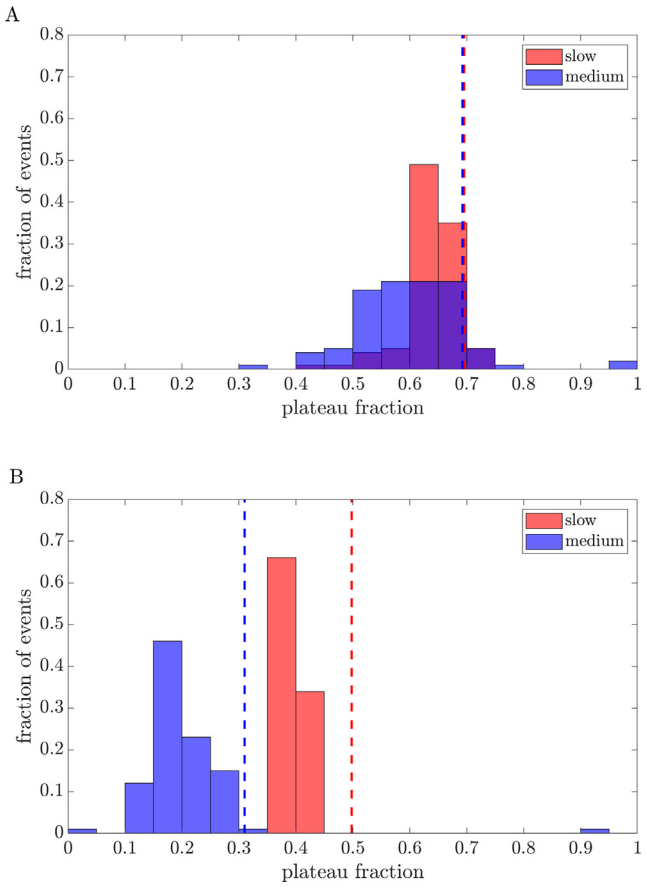

Fig. 11. Histograms of plateau fraction for noisy medium (blue) and slow (red) bursts, along with values for the deterministic cases (dashed). The plateau fraction is typically smaller for a noisy burst than for a deterministic one. (A) Histograms for the minimal β-cell model with parameter values as in Fig. 1. (B) Histograms for the IOM with parameter values as in Fig. 3. (For interpretation of the references to colour in this figure legend, the reader is referred to the web version of this article.)

(used in all previous IOM simulations) to 0.03 μM/ms, the system produces intrinsic glycolytic oscillations and slow bursting with $g_{K(Ca)} = 100$ pS. This slow bursting is characterized by pulses of the metabolite FBP (Fig. 12A), in contrast to the slow bursting analyzed above where the FBP timecourse has a triangle shape (Fig. 12B). (See McKenna and Bertram, 2018 for a description of the mechanisms driving these different types of oscillations.) This allows us to compare the effects of noise on slow bursting in the IOM driven by active metabolic oscillations to the effects in the same model, but where the slow bursting is driven by Ca^{2+} feedback and metabolic oscillations are passive. The effects of noise with passive metabolic oscillations have been shown earlier, in Fig. 4. For comparison, the effects of the same level of noise on the IOM with the larger v_{PDH} value is shown in Fig. 13. We see that, in both cases, active and silent phase durations are much less affected by noise during slow bursting than medium bursting. This is in spite of the fact that slow bursting is produced through a phantom bursting mechanism in Fig. 4 and intrinsic glycolytic oscillations in Fig. 13. (Medium bursting is driven by a phantom bursting mechanism in both cases.) Thus, we conclude that the existence of slow bursting in a noisy environment does not distinguish between slow burst mechanisms.

7. Discussion

We have demonstrated that slow bursting generated by the Integrated Oscillator Model for pancreatic β-cells in phantom bursting mode is much less sensitive to current noise than is medium bursting generated by the same model. This is in contrast to a much simpler phantom bursting model, where current noise affects both types of bursting about equally. There are important biological ramifications of this finding, since it tells us that the slow bursting observed in single β-cells could be due to a phantom bursting mechanism. It has been demonstrated previously that the slow bursting in single β-cells could also be due to intrinsic glycolytic oscillations; in such a case the bursting is very robust to noise (Pedersen, 2007). Taken together, one can conclude that there are at least two very different dynamical mechanisms that are consistent with slow bursting in the presence of noise, and thus consistent with the slow bursting of noisy single β-cells. Why is this important, when single β-cells are only found in the laboratory? *In vivo*, β-cells are clustered together into islets of Langer-

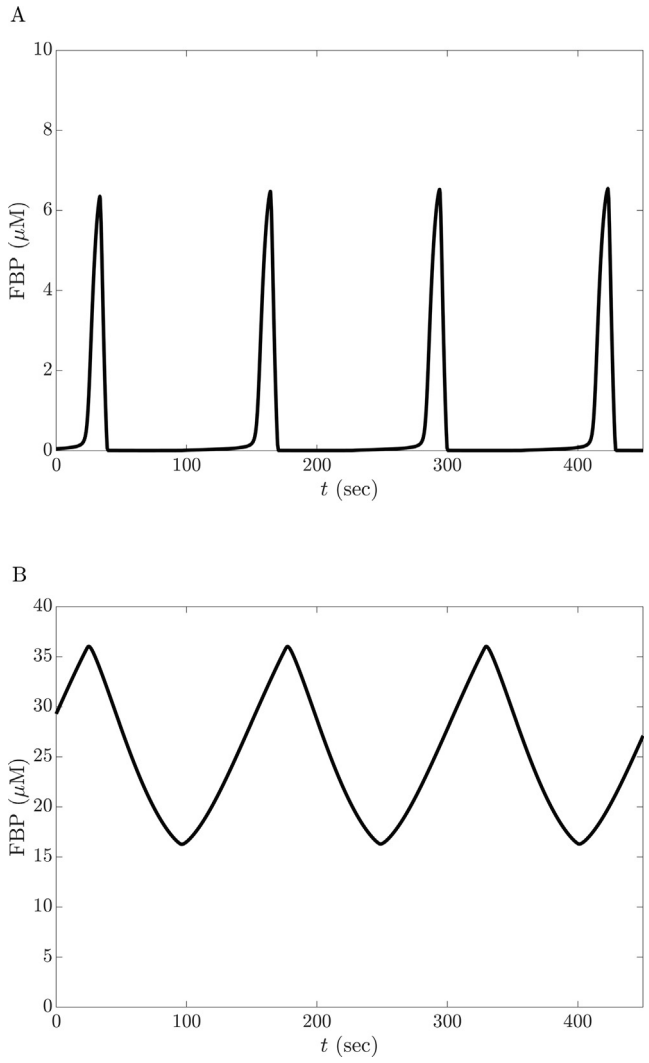

Fig. 12. Two different types of FBP oscilllations reflect different oscillation mechanisms (McKenna and Bertram, 2018). (A) FBP exhibits pulses when there is an active glycolytic oscillator. Produced when $v_{PDH} = 0.03$ μM/ms and $g_{K(Ca)} = 100$ pS. (B) The FBP timecourse has a triangle shape when metabolic oscillations are driven by Ca^{2+} feedback. Produced when $v_{PDH} = 0.002$ μM/ms and $g_{K(Ca)} = 100$ pS.

hans, with β-cells coupled to neighbors by gap junctions that provide electrical coupling, and for this reason the islet acts as a syncytium and the voltage trace of a β-cell in an islet is much less noisy than that from a β-cell removed from an islet (Kinard et al., 1999; Zhang et al., 2003). However, slow bursting in single β-cells, as reported in Jonkers et al. (1999), Zhang et al. (2003), Scarl et al. (2019), Smith et al. (1990), is still relevant because it is likely that the biological mechanism for these oscillations is the same in intact islets. Therefore, our work and that of Pedersen (2007) together suggest that slow bursting in islets could be due to either a phantom bursting mechanism or to intrinsic glycolytic oscillations. (They could of course also be due to a mechanism not examined in either study.).

There is a great deal of heterogeneity among single β-cells, in terms of gene expression (Dorrell et al., 2016), electrical activity (Kinard et al., 1999), Ca^{2+} dynamics (Zhang et al., 2003), and insulin secretion (Nasteska and Hodson, 2018). Coupling the cells together with gap junctions reduces the functional heterogeneity (Smolen et al., 1993), and a recent study showed that the glucose dose response curve for an islet is sharper than that for dispersed cells from an islet of the same mouse (Scarl et al., 2019). The same study showed that the plateau fraction of single β-cells is smaller than that of intact islets over the full range of glucose levels for which oscillations are produced (Scarl et al., 2019). This agrees with the prediction made with both the minimal phantom bursting model and the IOM (Fig. 11).

Phantom bursting refers to bursting in which the period is influenced by more than one slow variable, so that the burst period is not set by the time constant of any one variable (Bertram et al., 2000). In the minimal phantom bursting model used here the two slow variables are activation variables of K^+ channels whose properties were specified so as to produce a wide range of burst periods (Bertram et al., 2000). A more biophysical model was developed later, which had three slow variables, the cytosolic Ca^{2+} concentration, the Ca^{2+} concentration in the endoplasmic reticulum (ER), and a phenomenological variable for the ratio of the nucleotide adenosine diphosphate (ADP) to adenosine triphosphate (ATP) (Bertram and Sherman, 2004). We have examined the effect of current noise on medium and slow bursting produced by this model, and found that the noise dramatically shortens the medium bursting and has a more moderate effect on slow bursting (results not shown). The IOM builds on this model, and includes more biophysical elements such as a module for ATP production and consumption (Bertram et al., 2004), and we have shown here that slow bursting produced by the IOM is much less sensitive to noise than is medium bursting. Thus, a second result of our study is that the way in which the phantom bursting mechanism is implemented (i.e., the biophysical elements involved in the burst production) has a significant effect on the sensitivity of slow bursting to noise.

The IOM can produce slow bursting through two different mechanisms, depending on the choice of parameter values (Marinelli et al., 2018). In the first mode, analyzed in detail in McKenna and Bertram (2018), the slow oscillations are due to phantom bursting, with key roles played by the slow variation of ADP and the ER Ca^{2+} concentration, both of which reflect activity-dependent variation in the cytosolic Ca^{2+} concentration. In this mode metabolic oscillations are passive, responding to the rise and fall of cytosolic Ca^{2+} that occurs during bursting (Bertram et al., 2018). This is the mode primarily examined in the current study. In the second mode, there are intrinsic oscillations in glycolysis, which we refer to as active metabolic oscillations. This mode was the basis of slow oscillations in the Dual Oscillator Model that was used in the earlier study of noise by Pedersen (2007), which showed that noise had only a moderate effect on slow bursting. We found similar results in the IOM with parameters set to produce active metabolic oscillations; noise only moderately shortens the slow burst active and silent phases (Fig. 13), much like the effect of noise on slow bursting with passive metabolic oscillations (Fig. 4).

Given these two distinct mechanisms for slow bursting in β-cells, how can one determine which is valid? This question is the focus of ongoing investigations, and as of yet there is no definitive answer. One experimental study used a sensor for an enzyme activated by the glycolytic metabolite fructose 1,6-bisphosphate, and found that the sensor levels oscillated in a triangle-wave pattern during slow bursting. This provides evidence for slow bursting driven by passive metabolic oscillations (McKenna et al., 2016; Merrins et al., 2016). However, other experimental studies showed that metabolic oscillations can occur even when the cell's cytosolic Ca^{2+} level is not oscillating (Dryselius et al., 1994; Merrins et al., 2010), pointing to active metabolic oscillations that could be due

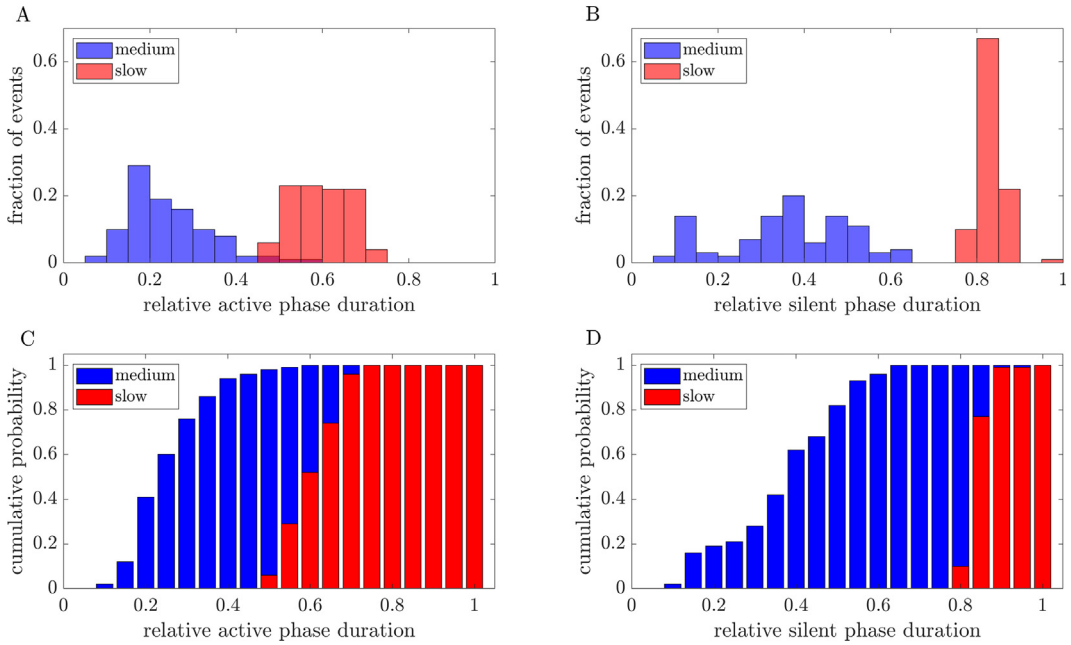

Fig. 13. Quantification of the effects of noise on medium and slow bursting in the Integrated Oscillator Model in which the slow bursting is due to intrinsic glycolytic oscillations. (A) Histogram of 100 events showing the active phase duration relative to that of the deterministic model. Medium bursting is shown in blue, while slow bursting is shown in red. (B) Histogram of 100 events showing the silent phase duration relative to that of the deterministic model. (C, D) Data from panels A and B plotted as cumulative probability distributions. In both cases, $v_{PDH} = 0.03$ μM/ms and noise is introduced by setting $\sigma = 300$ fA. For medium bursting $g_{K(Ca)} = 500$ pS and for slow bursting $g_{K(Ca)} = 100$ pS. (For interpretation of the references to colour in this figure legend, the reader is referred to the web version of this article.)

to oscillations in glycolysis. Indeed, it may be naive to expect that there is a unique mechanism for slow bursting in β-cells, given that slow insulin oscillations are normally found in non-diabetic humans as well as in dogs, rats, and mice. These oscillations facilitate the function of the liver in maintaining glycemic control (Matthews et al., 1983; Satin et al., 2015). Given the ubiquity and importance of slow insulin oscillations, which are driven by slow bursting oscillations, it should probably be expected that there are redundant mechanisms for their generation. The current study, together with Pedersen (2007), suggests that at least two mechanisms for slow bursting are consistent with studies of bursting in single β-cells.

CRediT author statement

Mehran Fazli: Conceptualization, Formal analysis, Investigation, Methodology, Software, Visualization, Writing-review & editing. **Theodore Vo:** Conceptualization, Formal analysis, Funding acquisition, Investigation, Methodology, Validation, Visualization, Writing-review & editing. **Richard Bertram:** Conceptualization, Formal analysis, Funding acquisition, Investigation, Methodology, Validation, Visualization, Writing-original draft.

Declaration of Competing Interest

The authors declare that they have no known competing financial interests or personal relationships that could have appeared to influence the work reported in this paper.

Acknowledgement

This work was partially supported by NSF grant DMS 1853342 to R. B. and T. V.

Appendix A. The minimal phantom bursting model

The minimal phantom model is described in detail in Bertram et al. (2000). Here, we give equations and refer the reader to Bertram et al. (2000) for a complete model description. The model is composed of four differential equations:

$$\frac{dV}{dt} = -(I_{Ca} + I_K + I_{s1} + I_{s2} + I_L + I_{noise})/C_m \tag{10}$$

$$\frac{dn}{dt} = \frac{n_\infty(V) - n}{\tau_n(V)} \tag{11}$$

$$\frac{ds_1}{dt} = \frac{s_{1\infty}(V) - s_1}{\tau_{s1}} \tag{12}$$

$$\frac{ds_2}{dt} = \frac{s_{2\infty}(V) - s_2}{\tau_{s2}} \,. \tag{13}$$

The ionic currents driving the dynamics of V are:

$$I_{Ca} = g_{Ca} m_\infty(V)(V - V_{Ca}) \tag{14}$$

$$I_K = g_K n(V - V_K) \tag{15}$$

$$I_{s1} = g_{s1} s_1 (V - V_K) \tag{16}$$

$$I_{s2} = g_{s1} s_2 (V - V_K) \tag{17}$$

$$I_L = g_L(V - V_L) \,. \tag{18}$$

The equilibrium activation and inactivation functions are:

$$m_\infty(V) = \frac{1}{1 + \exp((v_m - V)/S_m)} \tag{19}$$

$$n_\infty(V) = \frac{1}{1 + \exp((v_n - V)/S_n)} \tag{20}$$

$$s_{1,\infty}(V) = \frac{1}{1 + \exp((v_{s1} - V)/S_{s1})} \tag{21}$$

$$s_{2,\infty}(V) = \frac{1}{1 + \exp((v_{s2} - V)/S_{s2})} \tag{22}$$

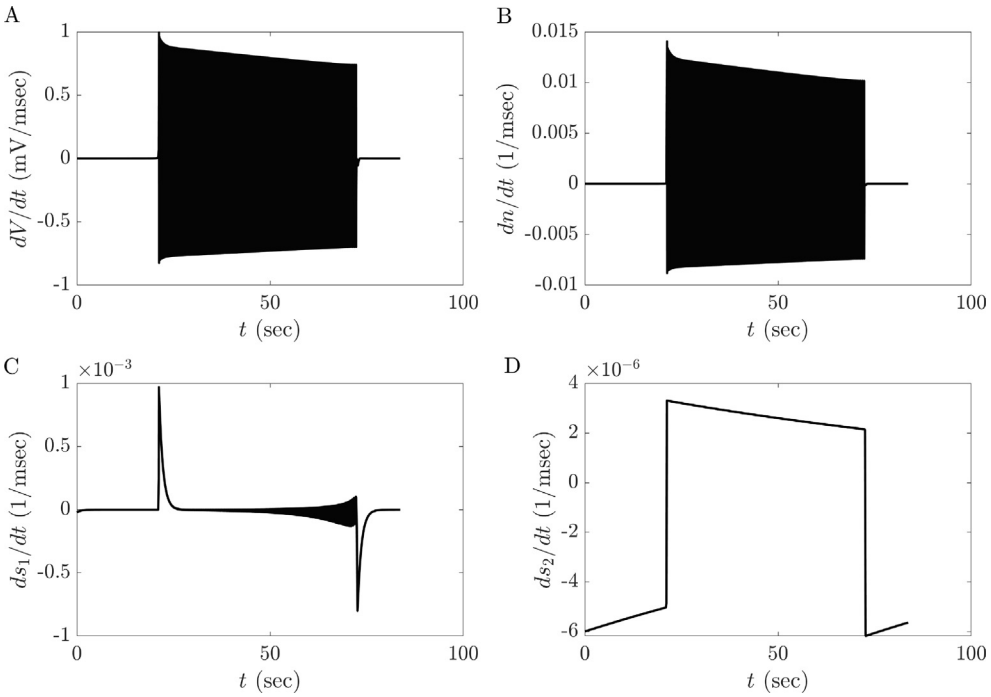

Fig. 14. Time-dependent derivatives of the four model variables during one slow burst (with $g_{s1} = 3$ pS). The derivatives for the V and n variables are much larger than those for the s_1 and s_2 variables, consistent with the classification of V and n as fast variables and s_1 and s_2 as slow variables.

Table 1
Parameters in the minimal phantom model.

Parameter	Value	Parameter	Value
C_m	4524 fF	v_m	−22 mV
g_{Ca}	280 pS	v_n	−9 mV
g_K	1300 pS	v_{s1}	−40 mV
g_L	25 pS	v_{s2}	−42 mV
g_{s1}	varies pS	S_m	7.5 mV
g_{s2}	32 pS	S_n	10 mV
V_{Ca}	100 mV	S_{s1}	0.5 mV
V_K	−80 mV	S_{s2}	0.4 mV
V_L	−40 mV	$\tau_{n,max}$	8.3 s
τ_{s1}	1 s	$v_{\tau n}$	9 mV
τ_{s2}	2 min	$S_{\tau n}$	10 mV

and the V-dependent time constant for n is:

$$\tau_n = \frac{\tau_{n,max}}{1 + \exp((V + v_{\tau n})/S_{\tau n})} . \tag{23}$$

In the body of the manuscript, we used a comparison of time constants for the model variables to justify the classification of V and n as fast variables and s_1 and s_2 as slow variables. Another way to do this would be to plot the derivatives of the variables and compare their magnitudes over a burst orbit. We do this in Fig. 14 for the case of slow bursting. The maximum derivatives of V and n are at least 10 times larger than those for s_1 and s_2, consistent with the classification of V and n as fast variables and s_1 and s_2 as slow variables (Table 1).

Appendix B. The Integrated Oscillator Model (IOM)

The IOM is described in detail in Marinelli et al. (2018). We give the model equations here, but refer the reader to Marinelli et al. (2018) for a full description. The model consists of eight differential equations:

$$\frac{dV}{dt} = -(I_{\mathrm{Ca}} + I_{\mathrm{K}} + I_{\mathrm{K(Ca)}} + I_{\mathrm{K(ATP)}})/C_m \tag{24}$$

$$\frac{dn}{dt} = \frac{n_\infty(V) - n}{\tau_n} \tag{25}$$

$$\frac{dc}{dt} = f_{\mathrm{Ca}}(J_{\mathrm{mem}} - J_{\mathrm{m}} - J_{\mathrm{er}}) \tag{26}$$

$$\frac{dc_{\mathrm{m}}}{dt} = f_{\mathrm{Ca}}\sigma_{\mathrm{m}}J_{\mathrm{m}} \tag{27}$$

$$\frac{dc_{\mathrm{er}}}{dt} = f_{\mathrm{Ca}}\sigma_{\mathrm{er}}J_{\mathrm{er}} \tag{28}$$

$$\frac{d\mathrm{F6P}}{dt} = 0.3(J_{\mathrm{GK}} - J_{\mathrm{PFK}}) \tag{29}$$

$$\frac{d\mathrm{FBP}}{dt} = J_{\mathrm{PFK}} - \frac{1}{2}J_{\mathrm{PDH}} \tag{30}$$

$$\frac{d\mathrm{ADP}}{dt} = \frac{\left\{\mathrm{ATP} - \exp\left[\left(1 + 2.2\frac{J_{\mathrm{PDH}}}{0.05+J_{\mathrm{PDH}}}\right)\left(1 - \frac{c}{0.35}\right)\right]\mathrm{ADP}\right\}}{\tau_a}. \tag{31}$$

Ionic currents are:

$$I_{Ca} = g_{Ca} m_\infty(V)(V - V_{Ca}) \tag{32}$$
$$I_K = g_K n(V - V_K) \tag{33}$$
$$I_{K(Ca)} = g_{K(Ca)} q_\infty(c)(V - V_K) \tag{34}$$
$$I_{K(ATP)} = g_{K(ATP)} o_\infty(\mathrm{ADP}, \mathrm{ATP})(V - V_K). \tag{35}$$

The equilibrium activation and inactivation functions are:

$$m_\infty(V) = \frac{1}{1 + \exp[(v_m - V)/s_m]} \tag{36}$$
$$q_\infty(c) = \frac{c^2}{k_d^2 + c^2} \tag{37}$$
$$o_\infty(\mathrm{ADP}, \mathrm{ATP}) = \frac{0.08 + 0.89\left(\frac{\mathrm{MgADP}}{k_{dd}}\right)^2 + 0.16\left(\frac{\mathrm{MgADP}}{k_{dd}}\right)}{\left(1 + \frac{\mathrm{MgADP}}{k_{dd}}\right)^2 \left(1 + \frac{\mathrm{ATP}^{4-}}{k_{tt}} + \frac{\mathrm{ADP}^{3-}}{k_{td}}\right)} \tag{38}$$
$$s_\infty(c_m) = \frac{c_m}{K_{PDH} + c_m}. \tag{39}$$

Here, $\mathrm{MgADP} = 0.165\mathrm{ADP}$, $\mathrm{ADP}^{3-} = 0.135\mathrm{ADP}$, and $\mathrm{ATP}^{4-} = 0.05\mathrm{ATP}$. The ADP and ATP concentrations are related by:

$$\mathrm{ATP} = \frac{1}{2}\left[A_{tot} + \sqrt{-4\mathrm{ADP}^2 + (A_{tot} - \mathrm{ADP})^2} - \mathrm{ADP}\right] \tag{40}$$

and A_{tot} is the total nucleotide concentration. Flux densities and reaction equations are:

$$J_{mem} = -\left[\frac{\alpha}{V_{cyt}} I_{Ca} + k_{PMCA} c\right] \tag{41}$$
$$J_{er} = k_{SERCA} c - p_{leak}(c_{er} - c) \tag{42}$$
$$J_m = k_{uni} c - k_{NaCa}(c_m - c) \tag{43}$$
$$J_{PFK} = v_{PFK} \frac{w_{1110} + k_{PFK} \sum_{i,j,l \in \{0,1\}} w_{ij1l}}{\sum_{i,j,k,l \in \{0,1\}} w_{ijkl}} \tag{44}$$
$$J_{PDH} = v_{PDH} s_\infty(c_m)\sqrt{\mathrm{FBP}} \tag{45}$$

where the w_{ijkl} are weights, given by:

$$w_{ijkl} = \frac{(\mathrm{AMP}/K_1)^i (\mathrm{FBP}/K_2)^j (\mathrm{F6P}/K_3)^k (\mathrm{ATP}/K_4)^l}{f_{13}^{ik} f_{23}^{jk} f_{41}^{il} f_{42}^{jl} f_{43}^{kl}} \tag{46}$$

where $\mathrm{AMP} = \frac{\mathrm{ADP}^2}{\mathrm{ATP}}$ (Table 2).

Table 2
Parameters used in the IOM.

Parameter	Value	Parameter	Value
C_m	5300 fF	p_{leak}	2×10^{-4} ms^{-1}
g_{Ca}	1000 pS	k_{uni}	0.4 ms^{-1}
g_K	2700 pS	k_{NaCa}	0.001 ms^{-1}
$g_{K(Ca)}$	varies pS	σ_m	100
$g_{K(ATP)}$	25000 pS	σ_{er}	31
V_{Ca}	25 mV	J_{GK}	0.001 μM ms^{-1}
V_K	−75 mV	v_{PFK}	0.01 μM ms^{-1}
v_m	−20 mV	k_{PFK}	0.06
s_m	12 mV	K_1	30 μM
v_n	−16 mV	K_2	1 μM
s_n	5 mV	K_3	5×10^4 μM
τ_n	20 ms	K_4	10^3 μM
k_d	0.5 μM	f_{13}	0.02
k_{dd}	17 μM	f_{23}	0.2
k_{tt}	1 μM	f_{41}	20
k_{td}	26 μM	f_{42}	20
f_{Ca}	0.01	f_{43}	20
α	5.18×10^{-18} μmol fA^{-1} ms^{-1}	v_{PDH}	varies μM ms^{-1}
V_{cyt}	1.15×10^{-12} l	K_{PDH}	200 μM
k_{PMCA}	0.2 ms^{-1}	τ_a	300000 ms
k_{SERCA}	0.4 ms^{-1}	A_{tot}	3000 μM

Appendix C. Supplementary data

Supplementary data associated with this article can be found, in the online version, at https://doi.org/10.1016/j.jtbi.2020.110346.

References

Atwater, I., Ribalet, B., Rojas, E., 1978. Cyclic changes in potential and resistance of the B–cell membrane induced by glucose in islets of Langerhans from mouse. J. Physiol. (Lond.) 278, 117–139.

Barbosa, R.M., Silva, A.M., Tomé, A.R., Stamford, J.A., Santos, R.M., Rosário, L.M., 1998. Control of pulsatile 5-HT/insulin secretion from single mouse pancreatic islets by intracellular calcium dynamics. J. Physiol. (Lond.) 510, 135–143.

Bergsten, P., 1995. Slow and fast oscillations of cytoplasmic Ca^{2+} in pancreatic islets correspond to pulsatile insulin release. Am. J. Physiol. 268, E282–E287.

Bertram, R., Previte, J., Sherman, A., Kinard, T.A., Satin, L.S., 2000. The phantom burster model for pancreatic β-cells. Biophys. J. 79, 2880–2892.

Bertram, R., Rubin, J., 2017. Multi-timescale systems and fast-slow analysis. Math. Biosci. 287, 105–121.

Bertram, R., Satin, L., Zhang, M., Smolen, P., Sherman, A., 2004. Calcium and glycolysis mediate multiple bursting modes in pancreatic islets. Biophys. J. 87, 3074–3087.

Bertram, R., Satin, L.S., Sherman, A.S., 2018. Closing in on the mechanisms of pulsatile insulin secretion. Diabetes 67, 351–359.

Bertram, R., Sherman, A., 2004. A calcium-based phantom bursting model for pancreatic islets. Bull. Math. Biol. 66, 1313–1344.

Chay, T.R., Keizer, J., 1983. Minimal model for membrane oscillations in the pancreatic β-cell. Biophys. J. 42, 181–190.

Cook, D.L., 1983. Isolated islets of Langerhans have slow oscillations of electrical activity. Metabolism 32, 681–685.

Cook, D.L., Crill, W.E., Porte Jr., D., 1980. Plateau potentials in pancreatic islet cells are voltage-dependent action potentials. Nature 286, 404–406.

Dorrell, C., Schug, J., Canaday, P.S., Russ, H.A., Tarlow, B.D., Grompe, M.T., Horton, T., Hebrok, M., Streeter, P.R., Kaestner, K.H., Grompe, M., 2016. Human islets contain four distinct subtypes of β cells. Nat. Commun. 7. https://doi.org/10.1038/ncomms11756.

Dryselius, S., Lund, P.-E., Gylfe, E., Hellman, B., 1994. Variations in ATP-sensitive K^+ channel activity provide evidence for inherent metabolic oscillations in pancreatic β-cells. Biochem. Biophys. Res. Commun. 205, 880–885.

Henquin, J.C., Meissner, H.P., Schmeer, W., 1982. Cyclic variations of glucose-induced electrical activity in pancreatic β-cells. Pflügers Arch. 393, 322–327.

Jonkers, F.C., Jonas, J.-C., Gilon, P., Henquin, J.-C., 1999. Influence of cell number on the characteristics and synchrony of Ca_{2+} oscillations in clusters of mouse pancreatic islet cells. J. Physiol. (Lond.) 520, 839–849.

Kinard, T.A., de Vries, G., Sherman, A., Satin, L.S., 1999. Modulation of the bursting properties of single mouse pancreatic β-cells by artificial conductances. Biophys. J. 76, 1423–1435.

Marinelli, I., Vo, T., Gerardo-Giorda, L., Bertram, R., 2018. Transitions between bursting modes in the integrated oscillator model for pancreatic β-cells. J. Theor. Biol. 454, 310–319.

Matthews, D.R., Naylor, B.A., Jones, R.G., 1983. Pulsatile insulin has greater hypoglycemic effect than continuous delivery. Diabetes 32, 617–621.

McKenna, J.P., Bertram, R., 2018. Fast-slow analysis of the integrated oscillator model for pancreatic β-cells. J. Theor. Biol. 457, 152–162.

McKenna, J.P., Ha, J., Merrins, M.J., Satin, L.S., Sherman, A.S., Bertram, R., 2016. Ca^{2+} effects on ATP production and consumption have regulatory roles on oscillatory islet activity. Biophys. J. 110, 733–742.

Meissner, H.P., Schmelz, H., 1976. Membrane potential of β-cells in pancreatic islets. Pflugers Arch. 351, 195–206.

Merrins, M.J., Fendler, B., Zhang, M., Sherman, A., Bertram, R., Satin, L.S., 2010. Metabolic oscillations in pancreatic islets depend on the intracellular Ca^{2+} level but not Ca^{2+} oscillations. Biophys. J. 99, 76–84.

Merrins, M.J., Poudel, C., McKenna, J.P., Ha, J., Sherman, A., Bertram, R., Satin, L.S., 2016. Phase analysis of metabolic oscillations and membrane potential in pancreatic β-cells. Biophys. J. 110, 691–699.

Nasteska, D., Hodson, D.J., 2018. The role of beta cell heterogeneity in islet function and insulin release. J. Mol. Endocrinol. 61, R43–R60.

Nunemaker, C.S., Bertram, R., Sherman, A., Tsaneva-Atanasova, K., Daniel, C.R., Satin, L.S., 2006. Glucose modulates $[Ca^{2+}]_i$ oscillations in pancreatic islets via ionic and glycolytic mechanisms. Biophys. J. 91, 2082–2096.

Nunemaker, C.S., Zhang, M., Wasserman, D.H., McGuinness, O.P., Powers, A.C., Bertram, R., Sherman, A., Satin, L.S., 2005. Individual mice can be distinguished by the period of their islet calcium oscillations: is there an intrinsic islet period that is imprinted in vivo? Diabetes 54, 3517–3522.

Pedersen, M.G., 2007. Phantom bursting is highly sensitive to noise and unlikely to account for slow bursting in β-cells: considerations in favor of metabolically driven oscillations. J. Theor. Biol. 248, 391–400.

Rorsman, P., Ashcroft, F.M., 2018. Pancreatic β-cell electrical activity and insulin secretion: of mice and men. Physiol. Rev. 98, 117–214.

Satin, L.S., Butler, P.C., Ha, J., Sherman, A.S., 2015. Pulsatile insulin secretion, impaired glucose tolerance and type 2 diabetes. Mol. Aspects Med. 42, 61–77.

Scarl, R.T., Corbin, K.L., Vann, N.W., Smith, H.M., Satin, L.S., Sherman, A., Nunemaker, C.S., 2019. Intact pancreatic islets and dispersed beta-cells both generate

intracellular calcium oscillations but differ in their responsiveness to glucose. Cell Calcium 83, 102081.
Sherman, A., Rinzel, J., Keizer, J., 1988. Emergence of organized bursting in clusters of pancreatic β-cells by channel sharing. Biophys. J. 54, 411–425.
Smith, P.A., Ashcroft, F.M., Rorsman, P., 1990. Simultaneous recordings of glucose dependent electrical activity and ATP-regulated K^+-currents in isolated mouse pancreatic β-cells. FEBS Lett. 261, 187–190.
Smolen, P., Rinzel, J., Sherman, A., 1993. Why pancreatic islets burst but single β-cells do not: the heterogeneity hypothesis. Biophys. J. 64, 1668–1679.
Tornheim, K., 1997. Are metabolic oscillations responsible for normal oscillatory secretion? Diabetes 46, 1375–1380.
Tornheim, K., Lowenstein, J.M., 1973. The purine nucleotide cycle. III. Oscillations in metabolite concentrations during the operation of the cycle in muscle extracts. J. Biol. Chem. 248, 2670–2677.
Tornheim, K., Lowenstein, J.M., 1974. The purine nucleotide cycle. IV. Interactions with oscillations of the glycolytic pathway in muscle extracts. J. Biol. Chem. 249, 3241–3247.
Valdeolmillos, M., Santos, R.M., Contreras, D., Soria, B., Rosario, L.M., 1989. Glucose-induced oscillations of intracellular Ca^{2+} concentration resembling bursting electrical activity in single mouse islets of Langerhans. FEBS Lett. 259, 19–23.
Watts, M., Tabak, J., Zimliki, C., Sherman, A., Bertram, R., 2011. Slow variable dominance and phase resetting in phantom bursting. J. Theor. Biol. 276, 218–228.
Yaney, G.C., Schultz, V., Cunningham, B.A., Dunaway, G.A., Corkey, B.E., Tornheim, K., 1995. Phosphofructokinase isozymes in pancreatic islets and clonal β-cells (INS-1). Diabetes 44, 1285–1289.
Zhang, M., Goforth, P., Bertram, R., Sherman, A., Satin, L., 2003. The Ca^{2+} dynamics of isolated mouse β-cells and islets: implications for mathematical models. Biophys. J. 84, 2852–2870.